https://doi.org/10.1016/j.jnucmat.2019.01.040
Journal of Nuclear Materials 517 (2019) 35 - 44

On the role of Ni, Si and P on the nanostructural evolution of FeCr alloys under irradiation

B. Gómez-Ferrer [a], C. Heintze [b], C. Pareige [a, *]

[a] Normandie Univ, UNIROUEN, INSA Rouen, CNRS, Groupe de Physique des Matériaux, 76000, Rouen, France
[b] Institute of Resource Ecology, Helmholtz-Zentrum Dresden - Rossendorf, Dresden, 01328, Germany

A B S T R A C T

In this experimental work the behaviour of Ni, Si and P, typical impurities or low alloying elements in ferritic/martensitic nuclear steels, with increasing irradiation dose was investigated in model FeCrX (X = Ni, Si, P, NiSiP) alloys using atom-probe 3D maps. These elements are known to increase the embrittlement and the hardening of steels by creating solute-rich clusters at 300 °C. This study is focused on the analysis of these clusters and the influence of every chemical specie in their formation. The model alloys have been irradiated with 5 MeV Fe^{2+} ions up to 0.1 and 0.5 dpa at 300 °C and the 3D atom maps have been analysed using statistical tools and iso-concentration algorithms. P is proven to be the fastest diffuser whereas Ni and Si are slower. The three species segregate together strengthening the idea that they are decorating stable defect clusters by dumbbell or vacancy dragging. And no apparent influence on the clustering of every element over the others is observed up to 0.1dpa, suggesting the absence of synergistic effect between these species.

1. Introduction

Comprehension of low-temperature embrittlement in irradiated ferritic/martensitic steels under irradiation is critical in order to push the operation temperature windows for future Gen IV and fusion reactor components designs. Part of the radiation embrittlement is caused by intragranular nanometric features, which induce hardening. In former works, hardening has been consistently explained in neutron irradiated model alloys whose purity was at an industrial level [1–3]. These FeCr model alloys, which had Cr concentrations ranging from 2.5 to 12 w%, contained also some impurities of Ni, Si and P. In these alloys, the increase in yield strength is linked to the presence of three reported types of small features: (i) dislocation loops detected by transmission electron microscopy (TEM) [4], (ii) solute-rich clusters (SRCs) observed by atom probe tomography (APT) and mainly enriched with Ni, Si, P and Cr [5,6] and (iii) Cr-rich clusters detected by APT and small angle neutron scattering (SANS) [5–8] which were identified as α' precipitates. After applying a disperse barrier hardening model, it turned out that the major contribution to the increase in yield strength was given by the SRCs and also by the α' particles in the case of Cr supersaturation [1,8]. The SRCs are systematically appearing in FeCr model alloys containing some Ni, Si or P impurities [5,6,9–12].

Pareige et al. [9] found strong indications that their formation is induced by the irradiation and not thermodynamically enhanced. These clusters could be either associated with small point defects clusters and/or with concentration fluctuations acting as traps for point defects. At 300 °C, P – very strongly — but also Ni and Si can migrate via vacancy dragging due to their strong solute-vacancy

* Corresponding author. GPM - UMR 6634 CNRS, Université de Rouen, Avenue de l'Université BP12, 76801 St. Étienne du Rouvray, France.
E-mail address: cristelle.pareige@univ-rouen.fr (C. Pareige).

https://doi.org/10.1016/j.jnucmat.2019.01.040

interaction energies (see Refs. [13–15] and references therein). Also the formation of P mixed interstitial atoms (MIAs) is energetically favourable [14,16] and the MIAs have even faster mobility than the self-interstitals (SIAs) in Fe [16,17]. Indeed a strong solute transport via interstitial dragging has been suggested as the dominant effect for the RIS of P whereas it is not expected for Si or Ni at this temperature [18]. Regarding Cr, it has a weak interaction with the vacancies [19–22] but a significant binding energy for SIAs [21,23,24] consequently the Cr atoms diffuse via vacancy and interstitial mechanism, the latter being at the origin of Cr dragging [18]. As a consequence, these species tend to segregate at dislocation loops and point defect sinks [5,10,11,25–35]. Comparison of the number density of TEM invisible dislocation loops obtained by Object Kinetic Monte Carlo (OKMC) simulations by Chiapetto et al. [36] with the number density of the SRCs measured by APT [5] make the assumption that SRCs are associated to small point defect clusters highly likely. Nevertheless, their formation mechanisms are not clear and a recent work from Bonny et al. [37] has discarded Ni-Cr synergistic effects as a possible formation mechanism. Since migrating P can be trapped by substitutional P atoms creating very stable complexes [14,16,38], it could be possible that these stable complexes act as a nuclei for the formation of the clusters.

The goal of this work is to study the influence of P, Ni and Si on the formation and the evolution of the radiation induced CrNiSiP-rich clusters in Fe-Cr alloys. In order to do so four Fe15%CrX alloys containing different diluted elements (X = Ni, Si, P, NiSiP) have been irradiated with Fe ions at two different doses. The irradiations were performed at a temperature of 300 °C and the samples have been investigated using APT. The distribution maps of the chemical species have been analyzed to characterize the evolution of the cluster's characteristics, i.e. size, number density, composition and size distribution, with the dose. The role of each chemical specie in the formation of the clusters is discussed. Cr also forms clusters which are not linked to SRCs at the higher dose in agreement with the work of Tissot et al. [39] but treatment of these clusters will not be addressed in this paper.

2. Materials and experiments

2.1. Materials

Four different FeCrX model alloys containing 15 at% Cr and different X chemical specie contents (X = Ni, Si, P, NiSiP) were cast by OCAS in an induction vacuum furnace. From each lab cast, the pieces were heat treated in a pre-heated furnace at 1200 °C for 1h30, subsequently hot rolled and finally air-cooled down to room temperature obtaining a fully ferritic microstructure (for further details see Ref. [40]). The final compositions, obtained from APT characterization at the present work are reported in Table 1.

2.2. Irradiation conditions

For the ion irradiations, the samples ($8-10 \times 10 \times 1\ mm^3$) were mirror polished before irradiation using mechanical polishing in several steps down to diamond suspension of 1 μm. Subsequently the deformed surface layer was removed by low-temperature (~0 °C) electropolishing using a solution of 98% of ethylen glycol monobutyl ether and 2% of perchloric acid.

The model alloys were irradiated with 5 MeV Fe^{2+} ions at 300 °C using a 3 MV-Tandetron accelerator at the Ion Beam Center of HZDR. All materials were irradiated to a nominal displacement damage of 0.1 dpa. Additionally one material (Fe15CrNiSiP) was irradiated to 0.5 dpa. The irradiation was designed in such a way that the nominal displacement damage was reached at a depth of 500 nm in order to avoid surface effect and the influence of the implantation peak [39]. The damage and implantation profiles given in Fig. 1 were calculated using SRIM (Stopping and Range of Ions in Matter) [41,42] with the "Quick Kinchin-Pease calculation" mode and using 40 eV as the displacement threshold for Fe [43] following the recommendation of Stoller et al. [44]. In order to guaranty a homogeneous lateral exposure over the whole set of samples the focussed ion beam was scanned over the area of the samples during the irradiation. The scanning frequencies were 1041 Hz and 1015 Hz in horizontal and vertical direction, respectively. The ion flux was measured continuously by means of Faraday cups (current measurement) and integrated to obtain the ion fluence. The ion flux was $1.3 \cdot 10^{11}\ cm^{-2} \cdot s^{-1}$ corresponding to a damage rate of $5 \cdot 10^{-5}$ dpa/s at 500 nm depth. The irradiation temperature of 300 °C was maintained by fixing the samples on a heating target. The temperature control was based on a thermocouple placed on the backside of one sample and no issue with T homogeneity is expected based on the design of the heater/holder system.

2.3. Atom probe technique and data analysis methods

For the characterization of the as-received (AR) materials, APT tips were electropolished using two different electrolytes: 75% acetic acid −25% perchloric acid and 98% ethylen glycol monobutyl ether − 2% perchloric acid, the latter being used as a final solution. After the irradiation, the APT tips were prepared by lift-out of a chunk and subsequent annular milling using a Scanning Electron Microscope − Focus Ion Beam (SEM-FIB ZEISS Crossbeam X540). At

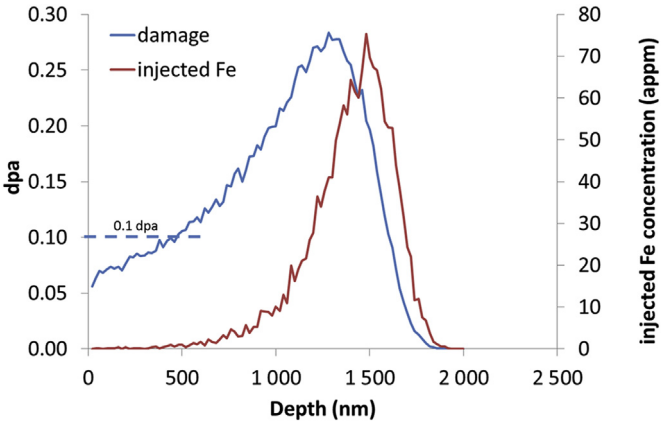

Fig. 1. Damage and injected Fe concentration profiles for the target dose 0.1 dpa at 500 nm.

Table 1
Intragranular compositions of the FeCrX (X = NiSiP, Ni, Si, P) model alloys measured by APT in at%.

Short Name	Cr (at%)	Ni (at%)	Si (at%)	P (at%)	Al (at%)	C (at%)	N (at%)
Fe15CrNiSiP	14.8 ± 0.4	0.098 ± 0.012	0.42 ± 0.05	0.065 ± 0.024	0.056 ± 0.004	0.011 ± 0.014	0.03 ± 0.02
Fe15CrNi	15.55 ± 0.11	0.099 ± 0.001	0.013 ± 0.013	0.003 ± 0.001	0.070 ± 0.001	0.010 ± 0.004	0.08 ± 0.02
Fe15CrSi	15.06 ± 0.18	0.006 ± 0.001	0.422 ± 0.019	0.002 ± 0.001	0.068 ± 0.001	0.006 ± 0.02	0.02 ± 0.03
Fe15CrP	15.0 ± 0.7	0.006 ± 0.01	0.016 ± 0.012	0.042 ± 0.002	0.064 ± 0.001	0.002 ± 0.001	0.01 ± 0.02

least three APT tips have been analysed for each condition. The APT volumes has been extracted from at least two or three different places guarantying different analysis of different grains. An APT volume corresponds to one analysed tip. Total volume analysed ranges from 0.3 to $1.6 \cdot 10^6$ nm^3 per conditions. All the tips were prepared at a depth of (500 ± 100) nm from the surface in order to investigate the regions of 0.1 dpa or 0.5 dpa. The final milling was performed with a Ga beam energy of 2 kV in order to reduce implantation of Ga ions in the material. The maximum concentration of Ga found in the samples did not exceed 0.05 at%.

APT acquisitions were made using a Local Electrode Atom Probe (LEAP 4000 XHR) from CAMECA. The samples were set at a temperature of 55K in order to avoid preferential evaporation of Cr atoms. The LEAP has a detector efficiency of 36% and provides a high mass resolution thanks to the presence of a reflectron. During the APT experiments the specimens were electrically pulsed with a pulse fraction of 20% at a pulse rate of 200 kHz. The detection rate was set up between 0.1% and 0.35%. Subsequently the APT volumes were reconstructed using IVAS 3.6.8 (CAMECA software). The reconstruction factors have been adjusted for every sample. The compression factor ξ has been systematically derived from the crystallographic angles between poles observed on the desorption maps and the field factor (k) has been derived from the expected interplanar distance at the poles. The values used for ξ and k have ranged between 1.3-1.8 and 2.8–6.4 respectively. The tip support (i.e. electropolished tip or tip on micro-coupon) has been noticed to influence the values of the reconstruction parameters (mainly k).

Finally the APT data treatment has been made using the 3D Software developed by the Groupe de Physique de Matériaux (GPM) in the University of Rouen Normandie, France. The analysis was oriented to study the distribution of the impurities (Ni, Si and P) in the matrix before and after irradiation. Since the dose was very low, the identification of SRCs was in some cases limited or not possible using iso-concentration algorithm [9,45]. Therefore in the present work, both the iso-concentration (also called iso-position method (IPM for short)) and a statistical tool based on the first near-neighbour distance distributions (1NN method) have been used in order to investigate the distribution of the low alloying components.

2.3.1. 1NN method

The frequency distributions of the 1NN distances of homo-pairs (X-X) or hetero-pairs (X-Y)— X or Y being either Ni, Si or P—have been measured experimentally for every APT volume in regions far away from field desorption lines and poles. To build the histograms the sampling size used was 0.05 nm. The frequency distributions have been softly smoothed by averaging over 3 successive points and normalized to 100. Analogous distance distributions were calculated for the same volumes after randomization of the atoms. In this case, the frequency distributions are fitted to a random distribution applying the model introduced by Philippe et al. [46] for diluted elements and summarized in equation (1):

$$P(r) = 4\pi r^2 Q C_0 \exp\left(-\frac{4}{3}\pi Q C_0 r^3\right) \quad (1)$$

Where $P(r)$ is the density probability to find two 1NN X atoms at a distance r within dr, Q is the detection efficiency and C_0 is the nominal concentration per unit of volume in the analysed volume.

From comparison of the experimental and randomized 1NN frequency distributions, early stages of clustering of low-concentration elements can be identified. The so called V parameter [47,48] has been used in order to compare the two distributions. In this work the V parameter is defined as indicated in equation (2):

$$V_{XY} = \sum_i \left| P_i^e - P_i^r \right| \quad (2)$$

where P_i^e and P_i^r are the experimental and random frequency distributions respectively. According to this definition, the V parameter measures the statistical distance between the random distribution of the pairs of the specified chemical species and their experimental distribution. It is used as a semi-quantitative parameter, which will allow making comparisons among the impurities distribution in the different materials and irradiation conditions.

2.3.2. Cluster characterization

The IPM is a cluster identification procedure based on three parameters: a concentration threshold (C_{th}) criterion, a minimum number of relevant atoms (Nb) detected in the clusters and a distance d corresponding to the distance below which two atoms belong to the same cluster ($d = 0.2$ nm) [45,49]. IPM calculations are performed on 3D concentration maps built from sampling of APT volumes in small boxes of 1 nm [49]. The selection of the parameters C_{th} and Nb is made in such a way that ghost clusters (i.e. clusters, which might be present in a random solid solution simply due to statistics) are avoided. C_{th} is ensuring that less than 0.01% of the filtered atoms in the random solution would have this concentration [45]. Finally, Nb is chosen in order to identify zero clusters in the random solution. These parameters were estimated for each APT volume. The IPM has been applied to the irradiated volumes at both irradiation conditions and SRCs have been identified. The parameters used for the IPM for the different materials and irradiation conditions are summarized in Table 2. For comparison purposes the samples at 0.5 dpa have been analysed with two different set of parameters, further explanations will be given in the results section.

The number density (N_V) of the identified clusters was determined by a simple ratio of the number of the observed clusters to the overall analysed volume. After application of cluster identification methods, clusters are often found to be surrounded by a matrix shell rich in Fe and Cr (matrix atoms in the vicinity of the clusters are erroneously associated to the clusters). These shells are systematically removed using an erosion method before measuring the size and the volume fraction. The radius of each cluster was calculated as indicated in equation (3) considering the clusters as spherical:

$$R_{clus} = \sqrt[3]{\frac{3nV_{at}}{4\pi Q}} \quad (3)$$

with n the number of atoms in each cluster, V_{at} the Fe atomic volume ($a_0^3/2$ with a_0 the lattice parameter) and Q the detector efficiency. This equivalent radius is calculated for every cluster and the average radius, R, is finally calculated and used as an indicator of the size of the clusters. The volume fraction (f_V) was defined as the ratio of the number of atoms inside the clusters to the total number of collected atoms. The cluster's composition was measured in the core of the clusters using erosion concentration profiles [49]. The cluster characteristics given by N_V, R, f_V and composition values were averaged over all the APT analysed volumes (at least 3 for each condition).

3. Results

The solute distributions obtained from the APT volumes are shown in Fig. 2 and Fig. 3. Already from visual inspection it is clear that the P atoms have grouped together after 0.1 dpa (Fig. 2(b)). It is

Table 2
Parameters used for IPM for every material at the different irradiation conditions. Concentration threshold has been applied either on X atoms (X = P, Si, Ni separately or Ni + Si + P). C_{th} corresponds to the threshold used for cluster detection Nb is the minimum number of X atoms in the clusters. It is also indicated whether or not clusters were identified using IPM.

Material	Method	Dose (dpa)	Element	C_{th} (at%)	Nb	Clusters detected
Fe15CrNi	IPM(Ni)	0.1	Ni	1.15–1.25	3–4	No
Fe15CrSi	IPM(Si)	0.1	Si	2.60–2.75	5–8	No
Fe15CrP	IPM(P)	0.1	P	1.35–1.45	3–4	Yes
Fe15CrNiSiP	IPM(Ni)	0.1	Ni	1.20–1.35	3–4	No
Fe15CrNiSiP	IPM(Si)	0.1	Si	2.50–2.65	5–7	No
Fe15CrNiSiP	IPM(P)	0.1	P	1.30–1.36	3–4	Yes
Fe15CrNiSiP	IPM(P)	0.5	P	1.36–1.46	3–4	Yes
Fe15CrNiSiP	IPM(NiSiP)	0.5	NiSiP	2.90–3.30	5–6	Yes

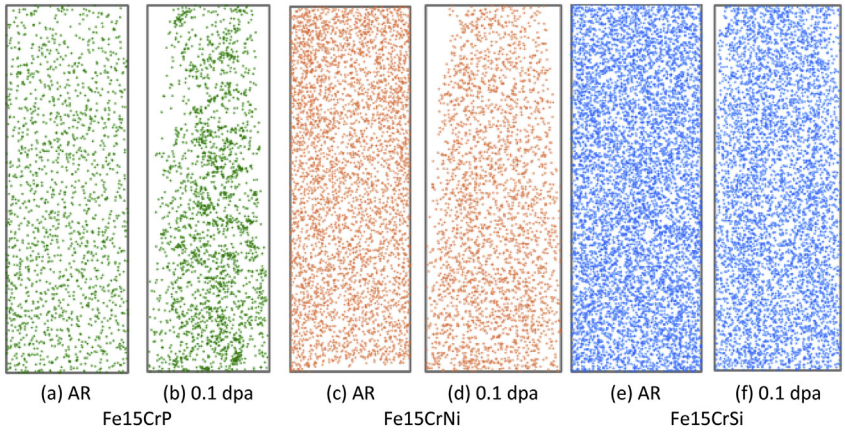

Fig. 2. Spatial distribution maps of chemical species in AR states and after 0.1 dpa ion irradiation at 300 °C: P (green dots), Ni (orange dots) and Si (blue dots) in (a) and (b) Fe15CrP — (c) and (d) Fe15CrNi —(e) and (f) Fe15CrSi. All the irradiated samples have been analysed at a depth of 500 ± 100 nm and the volumes shown here correspond to 40 × 40 × 120 nm^3. (For interpretation of the references to colour in this figure legend, the reader is referred to the Web version of this article.)

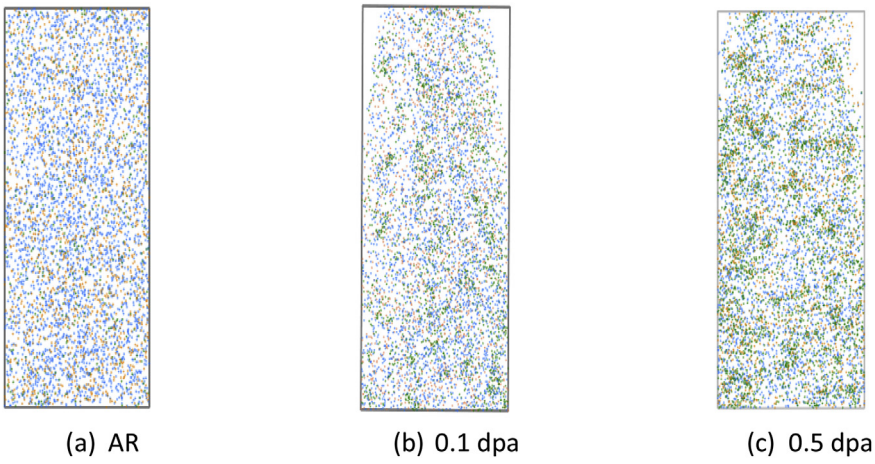

Fig. 3. Spatial distribution maps of chemical species: P (green dots), Ni (orange dots) and Si (blue dots) in Fe15CrNiSiP at different irradiations conditions: (a) AR, (b) 0.1 dpa at 300 °C and (c) 0.5 dpa at 300 °C. All the irradiated samples have been analysed at a depth of 500 ± 100 nm and the volumes shown here correspond to 40 × 40 × 80 nm^3. (For interpretation of the references to colour in this figure legend, the reader is referred to the Web version of this article.)

not the case for both Ni and Si atoms in Fig. 2(d) and (f); a clear rearrangement cannot be stated just by visual analysis. In the case of the model alloy containing the three types of impurities, the presence of clusters clearly enriched in P can be observed after 0.1 dpa in Fig. 3(b). At higher dose, 0.5 dpa, SRCs enriched in Ni, Si and P are visible as it is shown in Fig. 3(c).

Looking for a further quantitative and qualitative description of the chemical specie maps, the 1NN distances distributions have been determined and the *V* parameter has been calculated according to equation (2) for every Fe15CrX (X = Ni, Si, P, NiSiP) model alloy for the AR and both ion-irradiated conditions. The X-X and X-Y experimental and random 1NN frequency distance distributions are shown in Fig. 4 and Fig. 5 for the 0.1 dpa and 0.5 dpa conditions respectively. X-X 1NN distribution presented in Fig. 4(a) reports the distribution of the distances between X atoms. The distance between two X atoms will depend on the X concentration. The lowest

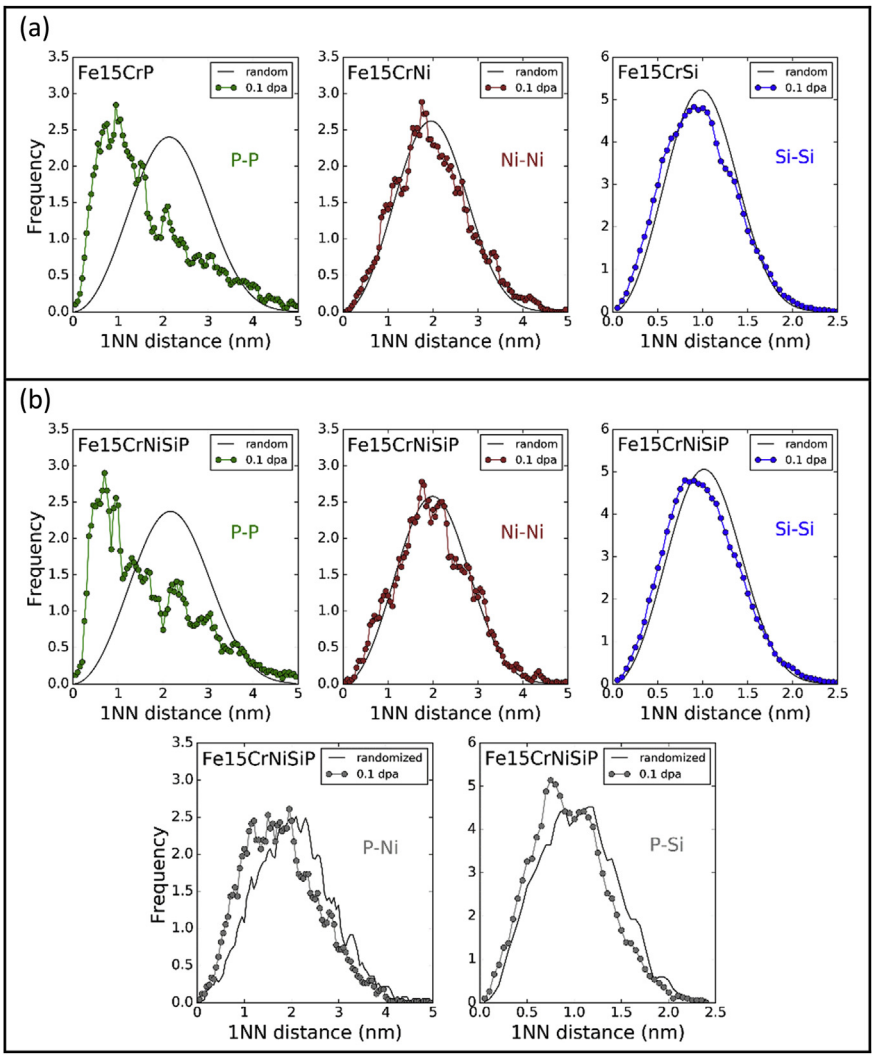

Fig. 4. (a) Normalized distribution of 1NN distances of X-X pairs in 0.1 dpa irradiated Fe15CrP, Fe15CrNi and Fe15CrSi. (b) Distributions of X-X and X-Y solute pairs in Fe15CrNiSiP model alloy irradiated up to 0.1dpa at 300 °C.

the concentration is, the larger is the distance. Si has the highest concentration (~0.4 at%) so the distance between Si atoms is the smallest: the peak of the random distribution is around 1 nm. The P concentration is much lower (~0.05 at%) so the distance between P atoms is larger than the distance between two Si. The peak of P-P 1NN random distribution is around 2 nm. Ni has an intermediate content (~0.1 at.%) but because of isotopic overlap with $^{58}Fe^{2+}$ or $^{31}P^{+}$, only the $^{60}Ni^{2+}$ (26% of natural abundance) peak has been considered for 1NN calculations. So the effective concentration for 1NN construction is 0.026 at.%. Consequently, the 1NN distances in the random distribution between Ni atoms are larger than the ones for P and Si. The X-Y distributions present the distribution of the distance of the X atoms around the Y atoms.

The 1NN distance distributions in the AR samples confirmed that the solutes are randomly distributed (not presented here). At 0.1 dpa, the results shown in Fig. 4, (a) and (b), reveal strong clustering of the P atoms in agreement with the visual inspection of the 3D images: the proportion of short 1NN distances for P-P pairs is much larger after irradiation than in random solid solution for both Fe15CrP and Fe15CrNiSiP. Slight clustering is also evident for Si (Si-Si plots) in both Fe15CrSi and Fe15CrNiSiP, whereas it was not possible to see anything on the 3D images in Fe15CrSi. The P-Si graph, which evaluates the distance distribution of the P atoms around the Si atoms, reveals an increased proportion of P-Si short 1NN distances with respect to random solid solution thereby underlying the fact that P and Si cluster altogether. Clustering tendency is not so clear in the case of Ni-Ni pairs at low dose whatever the alloy. However, P-Ni graph in Fe15CrNiSiP reveals that P atoms are closer to Ni than in the random state. In conclusion, at 0.1 dpa, strong clustering of P atoms, which are not only closer to other P atoms but also to Ni and Si atoms in Fe15CrNiSiP, is observed. When increasing the dose to 0.5 dpa, clear tendencies of all the species (even Ni-Ni) to be closer to each other are recognized in Fe15CrNiSiP, Fig. 5.

The *V* parameters are plotted as a function of the studied specie (P-P, Ni-Ni or Si-Si) and of the irradiation condition (AR, 0.1 or 0.5 dpa) in Fig. 6. Every dot corresponds to a different AP tip analysed, so the dispersion on the experimental results is illustrated. Qualitatively, the higher the *V* parameter is, the more deviated from the random distribution are the Ni, Si or P populations. It is important to notice that sensitivity of the *V* parameter depends on the nominal concentration of the studied element. This is because, as earlier explained in this section, the more diluted the element is, the larger the 1NN average distance will be and thus if short distances appear

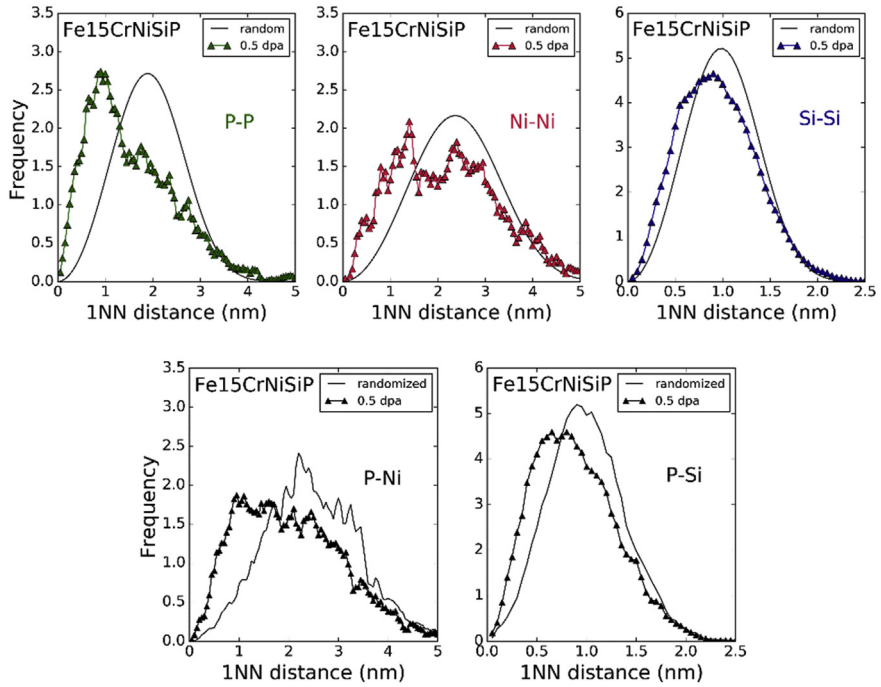

Fig. 5. Normalized distribution of 1NN distances of X-X and X-Y pairs in Fe15CrNiSiP model alloy irradiated up to 0.5dpa at 300 °C.

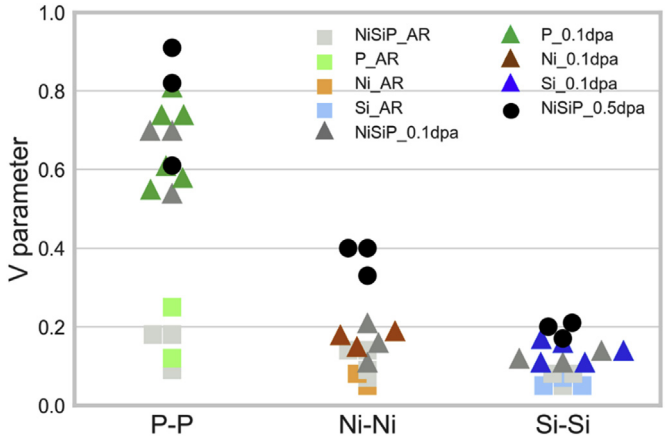

Fig. 6. V-parameter obtained from 1NN distributions of X-X pairs, X = (P, Ni, Si). AR results (squares), 0.1 dpa (triangles) and 0.5 dpa (circles) are plotted. The studied samples are Fe15CrP, Fe15CrNi, Fe15CrSi and Fe15CrNiSiP. Dots of the same colour represent different APT volumes analysed. (For interpretation of the references to colour in this figure legend, the reader is referred to the Web version of this article.)

due to clustering then the measured *V* parameter will be larger in the case of more diluted elements than in the case of higher nominal concentration.

Fig. 6 is indicating, how the P atoms are forming clusters. Interestingly, it appears from Fig. 6 that P clustering seems to almost saturate at 0.1 dpa given that no significant increase in the *V* parameter is found between 0.1 and 0.5 dpa for P-P pairs. In the case of Ni and Si, values of the *V* parameter at 0.1 dpa indicate that the solute distributions start to slightly deviate from the random as already pointed out by the 1NN plots. For Ni, a clear increase of clustering with dose is observed. For Si it is more difficult to conclude from the *V* parameter analysis due to the small variations in *V*. Irrespective of whether Ni, Si and P are alone or altogether in the alloys, the *V* parameter has the same values at the 0.1 dpa condition. According to these results, the behaviour of P is identical in both Fe15CrP and Fe15CrNiSiP regardless of the presence of Ni and Si. Similarly, Ni and Si clustering does not seem to be enhanced by the strong clustering tendency of P. Nevertheless, investigation of Fe15CrNi and Fe15CrSi irradiated at 0.5 dpa should be done to confirm this observation as the signals at 0.1 dpa are very low.

The cluster analysis using IPM has been performed for every irradiated model alloy as indicated in Table 2. As it can be seen in Table 2 a different set of parameters are chosen for IPM depending on the chemical specie investigated by the algorithm. The variation of the parameters C_{th} and *Nb*, which are required to unavoidably identify irradiation clusters, is linked to the nominal concentration of the specie considered in every AP tip. When the IPM filter is applied to identify P-rich clusters it will be referred to as IPM(P). The IPM(P) has been applied to Fe15CrP at 0.1 dpa and to Fe15CrNiSiP at 0.1 and 0.5 dpa. As it is indicated in Table 2, using IPM(Ni) or IPM(Si) filters to identify Ni or Si clusters, does not enable to detect clusters at 0.1 dpa. This is because clusters at 0.1 dpa are probably too small and/or weakly enriched in Ni and Si (as it will be shown below) and are thus below the detection limit of the IPM tool. In the case of IPM(NiSiP) the atoms of Ni, Si and P are treated by the software as if they are all the same element, thus in practical terms this means that the software analyses the volume as if the three types of atoms would be only one element and thus the effective nominal concentration in the sample would be $C_{NiSiP} = C_{Ni}+C_{Si}+C_{P}$. The consequence is that the values of C_{th} and *Nb* are larger than in the case of IPM(P). The model alloy Fe15CrNiSiP at 0.5 dpa has been analyzed using two filters: IPM(P) and IPM(NiSiP). The former analysis would allow to make direct comparisons to the materials irradiated at 0.1 dpa, tracking in this way the effect of the irradiation dose. The later would better describe the actual cluster characteristics since the three chemical species are clustering at the same regions (this point would be further addressed at the end of this section).

The results obtained with these filters i.e. characteristics of the clusters (N_V, *R* and f_V), are presented in Fig. 7(a) and in Table 3 for

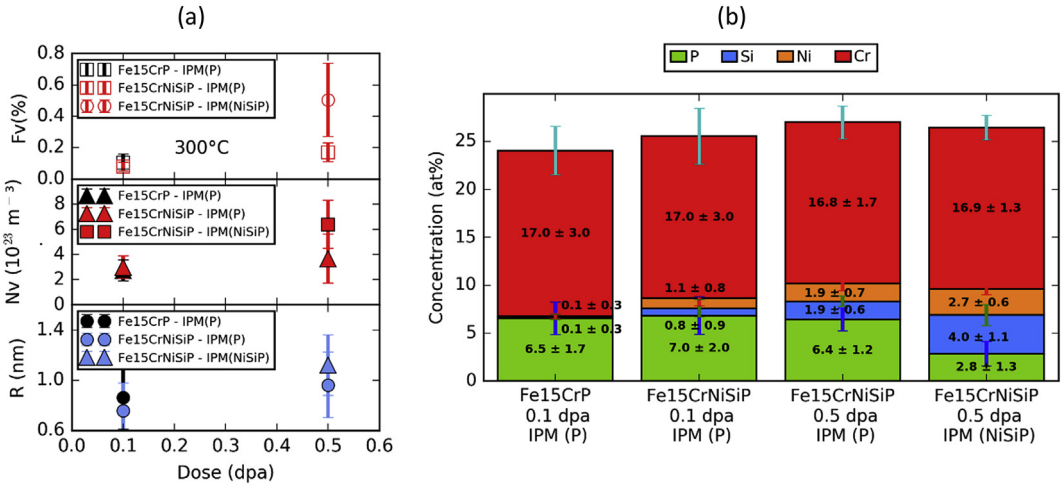

Fig. 7. Cluster characteristics of ion-irradiated specimens at 300 °C as a function of the dose a) volume fraction (fV), number density (NV) and radius (R) of the SRCs, b) solute concentration of the clusters. Fe concentration makes the balance to 100%.

Table 3
Characteristics of the SRCs measured by APT and analyzed with IPM.

Alloy	Dose (dpa)	IPM filter element	f_V (%)	N_V (10^{23} nm^{-3})	R (nm)
Fe15CrP	0.1	P	0.11 ± 0.05	2.7 ± 0.8	0.9 ± 0.3
Fe15CrNiSiP	0.1	P	0.08 ± 0.03	3.0 ± 0.9	0.8 ± 0.2
Fe15CrNiSiP	0.5	P	0.17 ± 0.06	3.7 ± 1.9	0.9 ± 0.3
Fe15CrNiSiP	0.5	NiSiP	0.61 ± 0.23	6.4 ± 1.9	1.1 ± 0.3

both 0.1 and 0.5 dpa. The characterization in terms of composition presented in Fig. 7(b) shows that in all cases the clusters are Fe-Cr based with a content of 17 at% of Cr and different Ni, Si and P contents depending on the material, the dose and the analysis method applied. Additionally, Fig. 8 presents the cluster size distributions. The size distributions are relevant in order to accurately characterize formed clusters since they provide information on the dispersion of the clusters size with respect to the averaged value.

3.1. 0.1 dpa – IPM(P)

At 0.1 dpa, Fig. 7 (a) shows that number density, size and volume fraction obtained using IPM(P) are very similar in both Fe15CrP and Fe15CrNiSiP alloys showing that the P cluster formation is not influenced by the presence of Ni and Si in the matrix. Fig. 7(b) which reports the SRC composition, shows that the P enrichment found at 0.1 dpa in both Fe15CrP and Fe15CrNiSiP after applying IPM(P) is the same. The SRCs found in the Fe15CrNiSiP alloy also

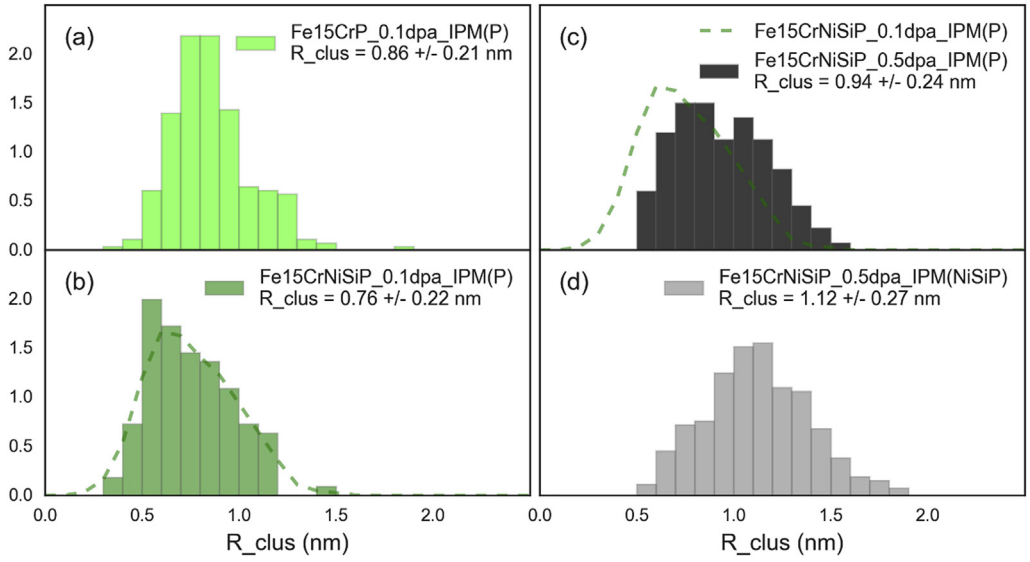

Fig. 8. Normalized size distributions of the SRCs obtained: (a) and (b) for Fe15CrP and Fe15CrNiSiP, respectively, at 0.1 dpa and (c) and (d) for Fe15CrNiSiP at 0.5 dpa using different sets of parameters, IPM(P) and IPM(NiSiP), respectively. The numbers of clusters used to build the histograms were (a) 280, (b) 110, (c) 133 and (d) 264. For comparison purpose, the dotted line plot in (c) represents the smoothed distribution of (b).

exhibit a presence of Ni and Si beyond their nominal concentration in compliance with the indications given by the *V* parameter and the 1NN curves.

3.2. 0.5 dpa – IPM(P)

At 0.5 dpa in the Fe15CrNiSiP, the results from Fig. 7(a) and Table 3 reveal that at higher dose, the detected P-rich clusters with IPM(P) present a slight increase in terms of f_V and N_v. The size distribution slips towards higher values as shown in Fig. 8(b and c). But because of the modification of the shape of the distribution, this only leads to a slight increase in average size (Table 3). The limited statistics on the size distributions do not allow to state further conclusions. Concerning the solute content of the clusters, a higher enrichment in Ni and Si is found (Fig. 7(b)) in good agreement with the 1NN analysis.

3.3. 0.5 dpa – IPM(NiSiP)

As it has been mentioned earlier in this section, the IPM(NiSiP) would better describe the actual characteristics of the SRCs formed; indeed, according to a visual inspection of the 3D APT datasets at 0.5 dpa, only considering P in the IPM is not correct since many clusters are missed in the identification. This indicates that some clusters are more diluted in P but richer in Si or Ni. These clusters are therefore only detected using IPM(NiSiP). Thus IPM(NiSiP) was also applied using the set of analysis parameters given in Table 2. As a consequence the detected f_V is three times bigger and N_v is almost double. The average size is larger, 1.1 nm, resulting from a displacement of the size distribution towards larger sizes (Fig. 8(d)). The larger average size of the clusters and the shift of the size distribution are likely to be due to the presence of Si and Ni atoms nearby the P atoms. Indeed, the average concentration of the clusters reveals even a stronger enrichment in Ni and Si than what was revealed with IPM(P) (see Fig. 7). With IPM(NiSiP) filter at 0.5 dpa, 73% of the SRCs identified are found enriched in Ni, Si and P, whereas 24% where found containing only Si and P and 3% only with Si. The fact that no P atoms were observed in the 3% of the clusters could be simply due to the detection efficiency of the APT (36%) and the small number of atoms concerned. This constrain also applies to the detection of Ni in the clusters. Another constraint for Ni is the fact that the identification on the 3D maps is only performed on the second isotope of Ni (26% of natural abundance) due to isotopic overlaps with $^{58}Fe^{2+}$ or $^{31}P^{+}$. Of course, isotopic overlaps are systematically corrected for composition measurements.

In every case—i.e. every combination of model alloy, dose and IPM analysis—no variation of SRCs' Cr content is observed with dose. Regarding the uncertainties, it is difficult to conclude on a Cr enrichment of the clusters. However it is worth noting that the measured Cr concentration is systematically 2% over the nominal one. This is coherent with Cr interstitial dragging mechanism and with experimental observations of Cr enrichment in SRCs under neutron irradiation [25] and Cr segregation at dislocation loops [11,31]. It must be emphasised that Cr-enriched clusters, which are not linked to SRCs, are observed at 0.5 dpa in agreement with the work of Tissot et al. [39]. Nevertheless, treatment of these clusters will not be addressed in this paper. The presence of C can also be noticed. This is linked to C contamination during irradiation. This contamination does not exceed 0.07 at.% and no significant amount of C was detected in the SRCs.

4. Discussion

In this work, it has been experimentally observed that the P-rich clusters are already formed at the lowest dose, 0.1 dpa, whereas not even Cr-rich clusters are observed. However, it is worth to note that the presence of Si or Ni enriched clusters cannot be ruled out because of the possible existence of very small cluster size/low concentrations at this dose in Fe15CrNi and Fe15CrSi. The analysis of the P-P *V* parameter evolution with dose indicates that clustering of P atoms is almost saturated at 0.5 dpa in sight of the smaller increase of the V-parameter at higher doses. P appears thus as the fastest diffuser and the specie having the strongest tendency to segregate. This is in full agreement with diffusion data [14,16] and the strongest dragging of P over the other elements predicted by Messina et al. [15,18], either via vacancy or interstitial mechanisms. Also, the high density of clusters and the saturation of the clustering agree well with the fact that P mixed dumbbells have been shown to create very stable complexes with substitutional P. This effect is likely to be at the origin of the increase of dislocation loop density in FeP alloys with respect to pure Fe [14,16,17,38]. These point defect sinks could be further enriched by dragging of P atoms via vacancies and interstitials.

From the concentration values of the SRCs at 0.1 dpa (Fig. 7 (b)) and from the analysis of the hetero-pairs, P-Ni and P-Si (Fig. 4(b)), it is clear that Ni and Si appear associated to the P-rich clusters. At the same time the values of *V* parameter, presented in Fig. 6, are similar for every X-X pair at 0.1 dpa independently of the presence of the respective other two elements in the alloy. Therefore, the clustering tendency of P does not seem to be modified by the presence of Ni and Si and the presence of P clusters is shown not to enhance Ni and Si clustering at 0.1 dpa. Thus from these results no synergetic effect has been detected between these species. However, the signal for Ni and Si is very small at 0.1 dpa in Fig. 6. In sight of these considerations further studies of Fe15CrNi, Fe15CrP and Fe15CrSi irradiated at 0.5 dpa would be required to confirm this conclusion since comparisons of the *V* parameter values and N_v could help to clarify whether the SRCs are stabilized by the presence of P or not.

The application of the IPM(P) to the Fe15CrNiSiP alloy allows to study the dose evolution on the SRCs under the same data treatment conditions and thus enabling direct comparisons to be made: at 0.5 dpa the P-rich clusters become richer in Si and Ni, accompanied by a slight increase in the number density. Therefore, according to a RIS process Si and Ni atoms, which are slower diffusers, reach the SRCs as the dose increases, also some more P atoms segregate at 0.5 dpa, but not as many as indicated by the saturation of the *V* parameter.

Further analysis of the clusters in the Fe15CrNiSiP alloy at 0.5 dpa using IPM(NiSiP) method, revealed that the SRCs are indeed more abundant, bigger, more diluted in P and more concentrated in Ni and Si than what could be detected by IPM(P). The fact that the correct identification of all the visible clusters is achieved by using IPM(-NiSiP) is another evidence that the three elements are segregating together in the same places. Still it is possible that the smallest SRCs are not detected, but this is the limitation of the analysis tool. We interpret the segregations of the three species at the SRCs as the decoration of stable point-defect clusters based on the experimental observations presented here and in previous works [9,36] as well as on the high affinity of these elements to segregate on dislocation loops and lines [5,11,15,25–30,33,34,34,35,37]. Segregation of these species at dislocation loops will have a strong impact on hardening since segregations can increase their obstacle strength [50,51].

5. Conclusions

The investigation into the role of Ni, Si and P in the cluster formation has been carried out by studying the model alloys Fe15CrNi, Fe15CrSi, Fe15CrP and Fe15CrNiSiP, both AR and ion-irradiated at 300 °C to 0.1 dpa (all) and 0.5 dpa (Fe15CrNiSiP only) using APT. It has experimentally observed that:

- P atoms have the strongest tendency to cluster. They are the fastest diffusers forming clusters at the lowest dose, 0.1 dpa.
- The P clustering is almost saturated at 0.1 dpa, since no significant increase of the *V* parameter is measured at 0.5 dpa.
- At 0.1 dpa, Ni and Si atom distributions are shown to slightly deviate from the random one indicating that they have a tendency to cluster but they diffuse more slowly.
- Even at low dose, P, Ni and Si are shown to cluster together.
- The f_V, N_V, R and the Ni, Si enrichment of the SRCs are increasing with the irradiation dose.
- *Results* indicate an absence of synergistic effects among Ni, Si and P in the formation of the SRCs. There is no indication that P, although being the faster diffuser and the specie having the strongest clustering tendency, influences the clustering of Ni and Si. This conclusion should be confirmed by further irradiations at higher dose.

Data availability

The raw/processed data required to reproduce these findings cannot be shared at this time as the data also forms part of an ongoing study.

Acknowledgements

This research was partly funded by the Euratom's Seventh Framework Programme FP7/2007–2013 under grant agreement No. 604862 (MatISSE project) and contributes to the EERA (European Energy Research Alliance) Joint Programme on Nuclear Materials (JPNM). Experiments were perfomed on the GENESIS platform. GENESIS is supported by the Région Haute-Normandie, the Métropole Rouen Normandie, the CNRS via LABEX EMC3 and the French National Research Agency as a part of the program "Investissements d'avenir" with the reference ANR-11-EQPX-0020. The use of the HZDR Ion Beam Center facilities and the support by its staff is gratefully acknowledged.

References

[1] F. Bergner, C. Pareige, M. Hernández-Mayoral, L. Malerba, C. Heintze, Application of a three-feature dispersed-barrier hardening model to neutron-irradiated Fe–Cr model alloys, J. Nucl. Mater. 448 (2014) 96–102, https://doi.org/10.1016/j.jnucmat.2014.01.024.

[2] M. Hernández-Mayoral, L. Malerba, M. Lambrecht, V. Kuksenko, C. Pareige, P. Pareige, F. Bergner, C. Heintze, A. Ulbricht, T. Toyama, M. Ramesh, B. Minov, M.J. Konstantinovic, Generation IV and Transmutation Materials (GETMAT) - Collaborative Project Seventh European Commission Framework Programme, Fission - 2007 -6.0.02 - Cross Cutting Topic: Materials Transmutation Technologies and Advanced Reactors, 2007.

[3] G. Monnet, Multiscale modeling of irradiation hardening: application to important nuclear materials, J. Nucl. Mater. 508 (2018) 609–627, https://doi.org/10.1016/j.jnucmat.2018.06.020.

[4] M. Hernández-Mayoral, C. Heintze, E. Oñorbe, Transmission electron microscopy investigation of the microstructure of Fe–Cr alloys induced by neutron and ion irradiation at 300 °C, J. Nucl. Mater. 474 (2016) 88–98, https://doi.org/10.1016/j.jnucmat.2016.03.002.

[5] V. Kuksenko, C. Pareige, P. Pareige, Cr precipitation in neutron irradiated industrial purity Fe–Cr model alloys, J. Nucl. Mater. 432 (2013) 160–165, https://doi.org/10.1016/j.jnucmat.2012.07.021.

[6] V. Kuksenko, C. Pareige, C. Genevois, F. Cuvilly, M. Roussel, P. Pareige, Effect of neutron-irradiation on the microstructure of a Fe–12at.%Cr alloy, J. Nucl. Mater. 415 (2011) 61–66, https://doi.org/10.1016/j.jnucmat.2011.05.042.

[7] F. Bergner, A. Ulbricht, C. Heintze, Estimation of the solubility limit of Cr in Fe at 300°C from small-angle neutron scattering in neutron-irradiated Fe–Cr alloys, Scripta Mater. 61 (2009) 1060–1063, https://doi.org/10.1016/j.scriptamat.2009.08.028.

[8] V. Kuksenko, Model Oriented Irradiation Experiments in Fe-Cr Model Alloys, Université de Rouen, 2011.

[9] C. Pareige, V. Kuksenko, P. Pareige, Behaviour of P, Si, Ni impurities and Cr in self ion irradiated Fe–Cr alloys – comparison to neutron irradiation, J. Nucl. Mater. 456 (2015) 471–476, https://doi.org/10.1016/j.jnucmat.2014.10.024.

[10] M. Bachhav, G. Robert Odette, E.A. Marquis, Microstructural changes in a neutron-irradiated Fe–15 at.%Cr alloy, J. Nucl. Mater. 454 (2014) 381–386, https://doi.org/10.1016/j.jnucmat.2014.08.026.

[11] M. Bachhav, L. Yao, G. Robert Odette, E.A. Marquis, Microstructural changes in a neutron-irradiated Fe–6 at.%Cr alloy, J. Nucl. Mater. 453 (2014) 334–339, https://doi.org/10.1016/j.jnucmat.2014.06.050.

[12] E.R. Reese, N. Almirall, T. Yamamoto, S. Tumey, G. Robert Odette, E.A. Marquis, Dose rate dependence of Cr precipitation in an ion-irradiated Fe 18Cr alloy, Scripta Mater. 146 (2018) 213–217, https://doi.org/10.1016/j.scriptamat.2017.11.040.

[13] G.J. Ackland, M.I. Mendelev, D.J. Srolovitz, S. Han, A.V. Barashev, Development of an interatomic potential for phosphorus impurities in -iron, J. Phys. Condens. Matter 16 (2004) S2629–S2642, https://doi.org/10.1088/0953-8984/16/27/003.

[14] C. Domain, C.S. Becquart, Diffusion of phosphorus in α-Fe: an ab initio study, Phys. Rev. B 71 (2005) 214109, https://doi.org/10.1103/PhysRevB.71.214109.

[15] L. Messina, M. Nastar, T. Garnier, C. Domain, P. Olsson, Exact ab initio transport coefficients in bcc Fe-X (X=Cr,Cu,Mn,Ni,P,Si) dilute alloys, Phys. Rev. B 90 (2014) 104203, https://doi.org/10.1103/PhysRevB.90.104203.

[16] E. Meslin, C.-C. Fu, A. Barbu, F. Gao, F. Willaime, Theoretical study of atomic transport via interstitials in dilute Fe – P alloys, Phys. Rev. B 75 (2007) 94303, https://doi.org/10.1103/PhysRevB.75.094303.

[17] H. Abe, E. Kuramoto, Interaction of solutes with irradiation-induced defects of electron-irradiated dilute iron alloys, J. Nucl. Mater. 271–272 (1999) 209–213, https://doi.org/10.1016/S0022-3115(98)00741-7.

[18] L. Messina, Multiscale Modeling of Atomic Transport Phenomena in Ferritic Steels, KTH Royal Institute of Technology, 2015.

[19] A. Benkaddour, O. Dimitrov, C. Dimitrov, Irradiation-induced defects in ferritic FeCr alloys, Mater. Sci. Forum (15–18) (1987) 1263–1268, https://doi.org/10.4028/www.scientific.net/MSF, 15-18.1263.

[20] A. Möslang, E. Albert, E. Recknagel, A. Weidinger, P. Moser, Interaction of vacancies with impurities in iron, Hyperfine Interact. 15 (1983) 409–412, https://doi.org/10.1007/BF02159779.

[21] P. Olsson, C. Domain, J. Wallenius, Ab initio study of Cr interactions with point defects in bcc Fe, Phys. Rev. B 75 (2007), https://doi.org/10.1103/PhysRevB.75.014110.

[22] O.I. Gorbatov, P.A. Korzhavyi, A.V. Ruban, B. Johansson, Y.N. Gornostyrev, Vacancy–solute interactions in ferromagnetic and paramagnetic bcc iron: ab initio calculations, J. Nucl. Mater. 419 (2011) 248–255, https://doi.org/10.1016/j.jnucmat.2011.09.002.

[23] T.P.C. Klaver, P. Olsson, M.W. Finnis, Interstitials in FeCr alloys studied by density functional theory, Phys. Rev. B 76 (2007), https://doi.org/10.1103/PhysRevB.76.214110.

[24] D. Terentyev, P. Olsson, L. Malerba, A.V. Barashev, Characterization of dislocation loops and chromium-rich precipitates in ferritic iron–chromium alloys as means of void swelling suppression, J. Nucl. Mater. 362 (2007) 167–173, https://doi.org/10.1016/j.jnucmat.2007.01.069.

[25] V. Kuksenko, C. Pareige, C. Genevois, P. Pareige, Characterisation of Cr, Si and P distribution at dislocations and grain-boundaries in neutron irradiated Fe–Cr model alloys of low purity, J. Nucl. Mater. 434 (2013) 49–55, https://doi.org/10.1016/j.jnucmat.2012.11.027.

[26] A.V. Barashev, Segregation of phosphorus atoms to grain boundaries in ferritic steels under neutron irradiation, Phil. Mag. Lett. 82 (2002) 323–332, https://doi.org/10.1080/09500830210135021.

[27] R.G. Faulkner, S. Song, P.E.J. Flewitt, M. Victoria, P. Marmy, Grain boundary segregation under neutron irradiation in dilute alloys, J. Nucl. Mater. 255 (1998) 189–209, https://doi.org/10.1016/S0022-3115(98)00022-1.

[28] A.V. Barashev, Monte Carlo simulation of phosphorus diffusion in alpha-iron via the vacancy mechanism, Philos. Mag. A 85 (2005) 1539–1555, https://doi.org/10.1080/14786430500036348.

[29] I.M. Neklyudov, V.N. Voyevodin, Features of structure-phase transformations and segregation processes under irradiation of austenitic and ferritic-martensitic steels, J. Nucl. Mater. 212–215 (1994) 39–44, https://doi.org/10.1016/0022-3115(94)90031-0.

[30] Z. Jiao, G.S. Was, Segregation behavior in proton- and heavy-ion-irradiated ferritic–martensitic alloys, Acta Mater. 59 (2011) 4467–4481, https://doi.org/10.1016/j.actamat.2011.03.070.

[31] A. Bhattacharya, E. Meslin, J. Henry, C. Pareige, B. Décamps, C. Genevois, D. Brimbal, A. Barbu, Chromium enrichment on the habit plane of dislocation loops in ion-irradiated high-purity Fe–Cr alloys, Acta Mater. 78 (2014) 394–403, https://doi.org/10.1016/j.actamat.2014.06.050.

[32] J.P. Wharry, G.S. Was, A systematic study of radiation-induced segregation in ferritic–martensitic alloys, J. Nucl. Mater. 442 (2013) 7–16, https://doi.org/10.1016/j.jnucmat.2013.07.071.

[33] M.K. Miller, K.A. Powers, R.K. Nanstad, P. Efsing, Atom probe tomography characterizations of high nickel, low copper surveillance RPV welds irradiated to high fluences, J. Nucl. Mater. 437 (2013) 107–115, https://doi.org/10.1016/j.jnucmat.2013.01.312.

[34] G. Bonny, D. Terentyev, E.E. Zhurkin, L. Malerba, Monte Carlo study of decorated dislocation loops in FeNiMnCu model alloys, J. Nucl. Mater. 452 (2014) 486–492, https://doi.org/10.1016/j.jnucmat.2014.05.051.

[35] C. Domain, C.S. Becquart, Solute – ⟨111⟩ interstitial loop interaction in α-Fe: a DFT study, J. Nucl. Mater. 499 (2018) 582–594, https://doi.org/10.1016/j.jnucmat.2017.10.070.

[36] M. Chiapetto, L. Malerba, C.S. Becquart, Effect of Cr content on the

nanostructural evolution of irradiated ferritic/martensitic alloys: an object kinetic Monte Carlo model, J. Nucl. Mater. 465 (2015) 326–336, https://doi.org/10.1016/j.jnucmat.2015.06.012.
[37] G. Bonny, A. Bakaev, P. Olsson, C. Domain, E.E. Zhurkin, M. Posselt, Interatomic potential to study the formation of NiCr clusters in high Cr ferritic steels, J. Nucl. Mater. 484 (2017) 42–50, https://doi.org/10.1016/j.jnucmat.2016.11.017.
[38] A. Hardouin-Duparc, Etude de la formation sous irradiation des amas de défauts ponctuels dans les alliages ferritiques faiblement alliés, PhD thesis, XI-Orsay University, Paris, 1998.
[39] O. Tissot, C. Pareige, E. Meslin, B. Décamps, J. Henry, Influence of injected interstitials on α′ precipitation in Fe–Cr alloys under self-ion irradiation, Mater. Res. Lett. 5 (2017) 117–123, https://doi.org/10.1080/21663831.2016.1230896.
[40] C. Pareige, C. Heintze, M. Hernandez-Mayoral, F. Bergner, B. Gómez-Ferrer, E. Onobre, M. Konstantinovic, E. Meslin, O. Tissot, B. Décamps, P. Desgardin, R. Coppola, L. Malerba, MatISSE FP7-Fission-2013, D.2.3.1. Microstructural and Mechanical Characterisation of Selected Ion and Neutron Irradiated Alloys, 2017.
[41] J.F. Ziegler, J.P. Biersack, U. Littmark, The Stopping and Range of Ions in Solids, Pergamon, 1985. https://books.google.es/books?id=xclwQgAACAAJ.
[42] J.F. Ziegler, SRIM-2003, Nucl. Instrum. Methods Phys. Res. Sect. B Beam Interact. Mater. At. 219–220 (2004) 1027–1036, https://doi.org/10.1016/j.nimb.2004.01.208.
[43] ASTM E693-12, Standard Practice for Characterizing Neutron Exposures in Iron and Low Alloy Steels in Terms of Displacements Per Atom (DPA), E 706(ID), ASTM International, West Conshohocken, PA, 2012, https://doi.org/10.1520/E0693-12. www.astm.org.
[44] R.E. Stoller, M.B. Toloczko, G.S. Was, A.G. Certain, S. Dwaraknath, F.A. Garner, On the use of SRIM for computing radiation damage exposure, Nucl. Instrum. Methods Phys. Res. Sect. B Beam Interact. Mater. Atoms 310 (2013) 75–80, https://doi.org/10.1016/j.nimb.2013.05.008.
[45] J.M. Hyde, G. DaCosta, C. Hatzoglou, H. Weekes, B. Radiguet, P.D. Styman, F. Vurpillot, C. Pareige, A. Etienne, G. Bonny, N. Castin, L. Malerba, P. Pareige, Analysis of radiation damage in light water reactors: comparison of cluster Analysis methods for the analysis of atom probe data, Microsc. Microanal. (2017) 1–10, https://doi.org/10.1017/S1431927616012678.
[46] T. Philippe, F. De Geuser, S. Duguay, W. Lefebvre, O. Cojocaru-Mirédin, G. Da Costa, D. Blavette, Clustering and nearest neighbour distances in atom-probe tomography, Ultramicroscopy 109 (2009) 1304–1309, https://doi.org/10.1016/j.ultramic.2009.06.007.
[47] P. Auger, A. Menand, D. Blavette, Statistical analysis of atom-probe data (ii) : theoretical frequency distributions for periodic fluctuations and some applications, J Phys C6 49 (1988) 439.
[48] D. Blavette, G. Grancher, A. Bostel, J Phys C6. 49 (1988) 433.
[49] W. Lefebvre, F. Vurpillot, X. Sauvage, Atom Probe Tomography - Put Theory into Practice, Elsevier Science, San Diego , 2016.
[50] D. Terentyev, A. Bakaev, Radiation-induced strengthening and absorption of dislocation loops in ferritic Fe–Cr alloys: the role of Cr segregation, J. Phys. Condens. Matter 25 (2013) 265702, https://doi.org/10.1088/0953-8984/25/26/265702.
[51] G. Bonny, A. Bakaev, D. Terentyev, E. Zhurkin, M. Posselt, Atomistic study of the hardening of ferritic iron by Ni-Cr decorated dislocation loops, J. Nucl. Mater. 498 (2018) 430–437, https://doi.org/10.1016/j.jnucmat.2017.11.016.